LABORATORY MULTISTATIC POLARIMETRIC SPARSE APERTURE 3D SAR INVESTIGATION

R Welsh Centre for Electronic Warfare, Information and Cyber, Cranfield University, Defence Academy of the United Kingdom, SN6 8LA, UK
D Andre Centre for Electronic Warfare, Information and Cyber, Cranfield University, Defence Academy of the United Kingdom, SN6 8LA, UK
M Finnis Centre for Defence Engineering, Cranfield University, Defence Academy of the United Kingdom, SN6 8LA, UK

1 INTRODUCTION

Synthetic Aperture Radar (SAR) is a coherent technique that produces high quality imagery, with a finer cross-range resolution than would be possible with a stationary antenna. Radar pulses from multiple points along a flight path are combined, with return time and phase recorded for each pulse[1]. This technique can be used to produce multidimensional 3D SAR images, with scatterers otherwise overlaid in range and azimuth separated out in height.

Producing 3D SAR imagery through conventional methods can be challenging for practical scenarios, due to the large scanning time required[2]. Separating scatterers in elevation typically requires many horizontal repeat-passes over a target scene, with a finely sampled 2D SAR aperture for the best results. A reduction in the data collection sampling in the vertical dimension will often cause a reduction in image quality, sacrificing either vertical resolution or a wide-swath coverage in the vertical dimension or vertical sidelobe quality[3].

Several methods have been developed for forming 3D SAR imagery from sparsely sampled aperture data sets each with their own limitations. Dual-pass SAR interferometry is a long-established technique in this area, forming scatterer height estimates of terrain from two horizontal passes. This method is unable to separate out scatterers overlaid in height along the same azimuth and range[4]. More recently developed methods include 3D SAR compressive sensing[5]. This method is highly dependent on the nature of the target scene and is also computationally expensive, achieving limited success thus far.

The SAR Point Cloud Generation System (SPCGS) was developed for producing sparsely sampled aperture 3D SAR imagery (3D point clouds), using a series of 2D SAR interferograms produced from horizontal SAR apertures with randomized heights to produce 3D scatterer information[6]. This method has shown promise, having been demonstrated on simulated SAR far-field monostatic target scenes, but is not applicable for SAR collects employing SAR near-field collection geometries or bistatic and multistatic geometries[7]. This is due to algorithm simplifying assumptions, including a constant grazing angle across the target scene. Furthermore, there is a lack of published literature regarding the algorithm performance on measured data.

We have generalized the SPCGS algorithm into a novel Sparse SAR Volumetric Interferometry (SSARVI) processing-based technique which produces 3D SAR imagery from sparsely sampled SAR aperture data, for bistatic, multistatic and SAR near-field target scenarios[8]. The motivation behind the development was to provide an image formation algorithm suitable for envisaged multistatic SAR collections from satellite constellations and UAV-SAR drone swarms[9,10,11]. The dependence of sidelobe height on the unevenness of SAR height spacing was explored through simulation, and high-quality sub-Nyquist 3D renderings were produced.

This paper presents preliminary research into the extension of the technique to include polarimetric data. Sparse aperture 3D-PolSAR methods are currently underdeveloped for bistatic and multistatic collection geometries. Data for this study was measured at the Cranfield GB-SAR laboratory.

This paper first describes the new volumetric sparse aperture imaging approach in section 2, describes the polarimetric decompositions investigated in section 3, presents 3D image results in section 4, and conclusions and discussion in section 5.

2 VOLUMETRIC SPARSE-APERTURE APPROACH

The new SSARVI approach[8], developed for bistatic and multistatic sparse-aperture 3D SAR, exploits volumetric processing. This accounts for distortions in layover caused by the challenging geometries, which can be SAR near-field, for example due to the grazing angle variation across the scene.

In the approach, N sparsely and unevenly distributed horizontal SAR aperture pass heights are employed to form N-1 volumetric interferograms. The uneven distribution prevents aliasing of signatures in the vertical direction. The phase factors of the interferograms are then coherently summed at each voxel position, for the sparsely sampled data set[8].

Each interferogram contributes a vertical iso-range arc of providing no resolution in elevation individually. However, when the interferograms are coherently summed, each arc crosses at the scatterer locations due to the use of volumetric processing causing a large amplitude coherent sum. The 3D coordinates of the scatterer locations can then be extracted by applying a threshold to the sum. A histogram-based approach is used to set the threshold, as is common in other image processing applications. The process is summarized as follows,

$$Det = \frac{1}{N}\left|1 + \Sigma_{n=1}^{N-1} e^{-i\varphi_n}\right| > Th \quad (1)$$

where *Det* are the detection voxel locations surpassing the threshold *Th*, N is the number of horizontal passes in SAR aperture and φ_n are the interferogram phases at each voxel location. The mean intensity from the N SAR volumetric images at each detection point can be applied to that position, which can sometimes improve the interpretability of the renderings[8].

3 SAR POLARIMETRY

SAR Polarimetry can provide useful extra scene information. Polarimetric techniques commonly employ the four linear polarisation channels HH, HV, VH and HV to form different polarimetric decompositions which can help classify scatterer types. The Pauli decomposition[12] provides a simple approach to roughly divide scatterer responses as Odd-bounce ray interactions, Even-bounce, and Cross-polarization. For example, spheres, flat plates, and trihedral corner reflectors tend to scatter brightly in the Odd-bounce decomposition and not in the Even or cross-polarization decompositions.

The Pauli decomposition can be presented with different colour schemes, associating the colours with the scattering components[13]. The three Pauli decomposition channels consist of coherent sums of the linear polarisation channels[12],

$$Odd = \frac{1}{\sqrt{2}}|HH + VV| \quad (2)$$

$$Even = \frac{1}{\sqrt{2}}|HH - VV| \quad (3)$$

$$Cross\ Polar = \sqrt{2}|HV| \quad (4)$$

It is noted that the “Pauli Even-bounce” component (2) can be combined with the linear cross polarisation component (4) for a more complete Even-bounce measure which can take into account rotated dihedral corner reflector signatures. It is also noted that in monostatic geometries, the two linear cross-polarisation channels are equivalent, however this is not the case for bistatic collections[14]. In multistatic collections, the physical meaning of these decompositions is less clear, however bistatic

generalisations have been developed[15,16,17] which have been implemented for 3D imaging of building interiors[18,19].

4 GBSAR LABORATORY

The experimental presented was collected at the Cranfield University Ground-Based SAR (GBSAR) laboratory. The GBSAR laboratory performs microwave measurements with a Vector Network Analyser (VNA), which generates a stepped frequency waveform. The system currently performs indoor measurements, with the VNA attached to two dual polarization Ultra-Wideband horn antennas capable of transmitting and receiving within the range 1-10 GHz. The Antennae can be arranged in a bistatic or a pseudo monostatic configuration.

Figure 1 shows a target scene being scanned by the antennae in a bistatic configuration. Here, each antenna is mounted on a different vertical two-dimensional SAR aperture scanner. The transmit SAR aperture is 3.5 m wide by 1.5 m high, and receive SAR aperture is 1.3 m wide by 1.5 m high.

When a SAR scene is left undisturbed, and transmitter trajectories are precisely repeated, the combination of repeat scans with the receiver in different locations (or trajectories) is equivalent to a multistatic scan with multiple receivers operating simultaneously. Using this approach, multistatic scans have been collected in the GBSAR lab, even though the VNA has only two ports.

The measured target scene consisted of a quarter scale T72 tank model placed on gravel and additional reference spheres. The gravel provides a SAR speckle clutter background, with shadowing visible, depending on SAR geometry.

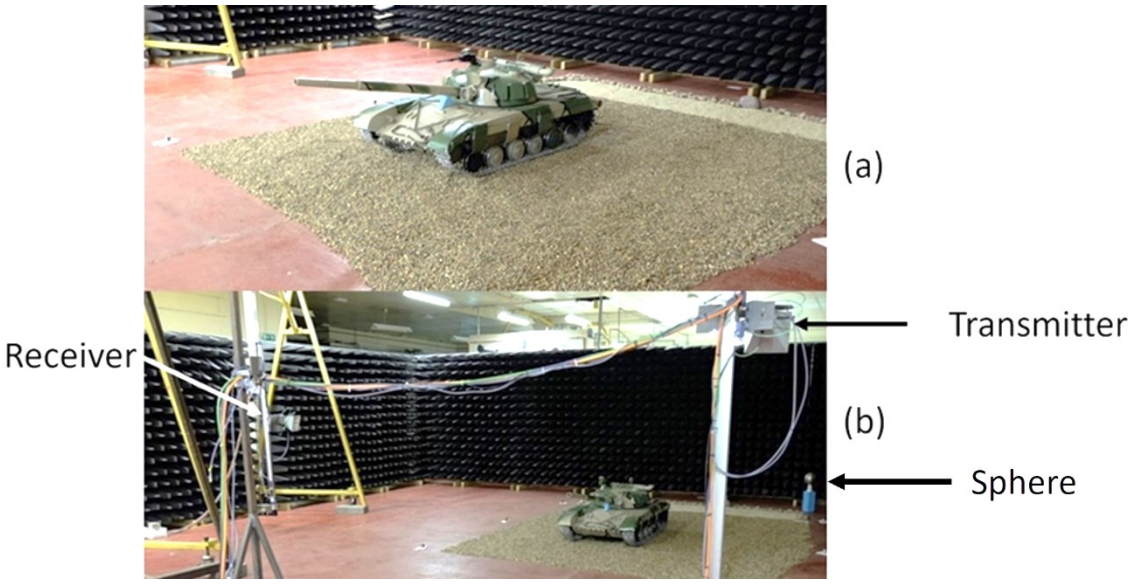

Figure 1. Images of lab scene, showing a quarter scale model tank (a), and the tank scene being scanned in a bistatic configuration (b) with the reference sphere.

Full Nyquist sampled 2D SAR apertures were collected and can be downsampled to test the performance of image formation algorithms with different sparse elevational sampling. Example sparse SAR geometries are shown in Figure 2, which are employed to generate the results in section 5.

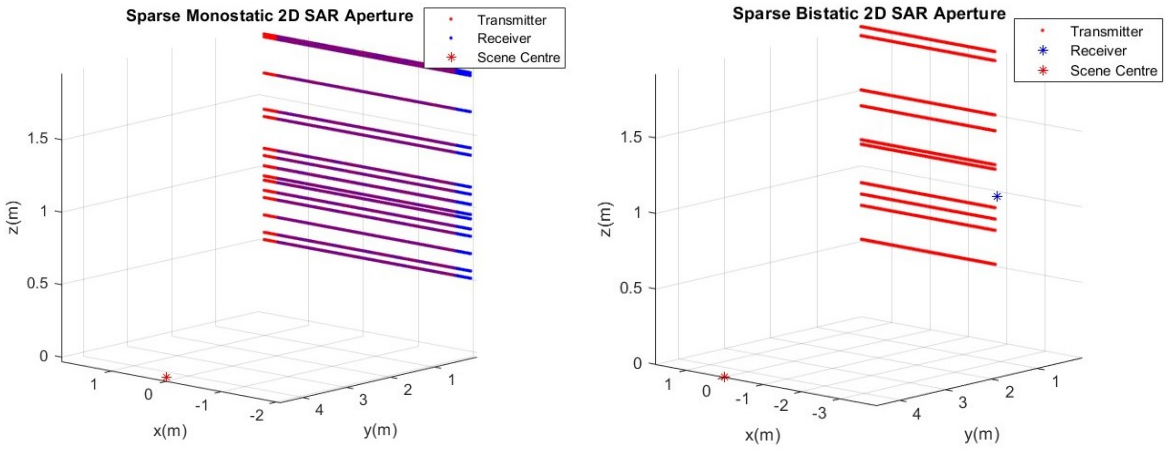

Figure 2. Geometries obtained from the GBSAR laboratory: sparsely-sampled monostatic (a) and bistatic (b) 2D SAR apertures.

The transmitter traverses the vertical aperture with the receiver either mounted on the same platform, as shown in Figure 2a), or positioned off to the side on the second axis, as shown in Figure2b) This means that downsampled apertures can be produced for both pseudo-monostatic and bistatic collection geometries.

5 RESULTS

Laboratory polarimetric SAR data was collected as described in section 4, providing four channels of linear polarization scattering amplitude data. Point cloud detections were performed with the SSARVI algorithm[8] upon separate linear polarization channels, or alternatively on the Pauli decompositions (2-4). Monostatic results are presented in section 5.1 and bistatic in 5.2. The SAR geometries used to generate the results in this section are displayed in Figure 2.

5.1 Monostatic

Figure 3 shows the point cloud detections from sampling a monostatic 2D SAR vertical aperture sub-Nyquist sampled in height. The detections for each polarisation channel are overlaid (note that the cross-polarization channels are equivalent in monostatic geometries).

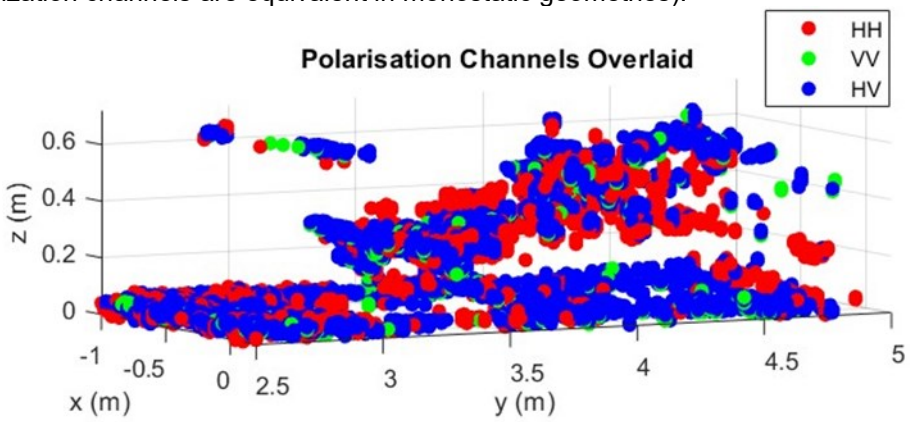

Figure 3. Sub-Nyquist point cloud detections, overlaid for each linear polarisation channel.

The sparse SAR aperture employed is shown in Figure 2a). It consists of 18 horizontal linear passes, necessarily unevenly distributed in height with a normalized standard deviation of 0.53. The aperture has a maximum inter-pass spacing of 25 cm, which would normally give a corresponding unambiguous vertical cross range of 32 cm. For a 1.8 m high Volume of Interest (VoI), this

corresponds to a vertical sampling rate of 36% below full Nyquist vertical sampling, assuming a uniformly sampled aperture. The SSARVI results show no vertical aliasing, which would be the case with images formed from conventional SAR image formation algorithms. Furthermore, erroneous detections are not evident.

In Figure 4, monostatic polarimetric decomposition sub-Nyquist aperture point cloud renderings are presented. These are formed for a cuboid volume containing the reference sphere visible in Figure 1b). The point cloud detections were associated with mean polarimetric decomposed scattering intensity, and projected along the horizontal cross-range direction (x-direction). The Pauli Odd and Even-bounce decompositions in (2) and (3) are associated with green and red colour maps respectively.

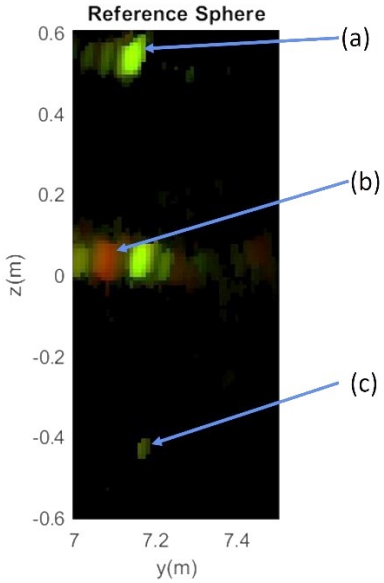

Figure 4. YZ-plane view (projection in the horizontal cross-range direction) of polarimetric decomposed sub-Nyquist aperture point cloud, showing the reference sphere and multipath artefacts. Green and red signatures correspond to Odd and Even-bounce decompositions respectively.

Several scatterer signatures are visible. The top-most, labelled (a) is the direct sphere response, and is Odd-bounce. At ground-level (z = 0 m) there is an Even-bounce signature (b) which may involve scattering from the ground followed by scattering from sphere (and reverse). The Odd-bounce signature at ground level may be some direct response from ground-clutter (stones). The bottom most signature is Odd-bounce and is the below-ground mirror image of the sphere response, involving two interactions with the ground and one with the sphere.

Figure 5 shows a polarimetric decomposed point cloud rendering of the model tank. The SSARVI algorithm is applied separately to all three Pauli decompositions (2-4), providing point clouds associated with each. The Odd-bounce decomposition is in green, and Even-bounce + Cross-Polarization are combined in red, and joint detections between these two sets are coloured blue.

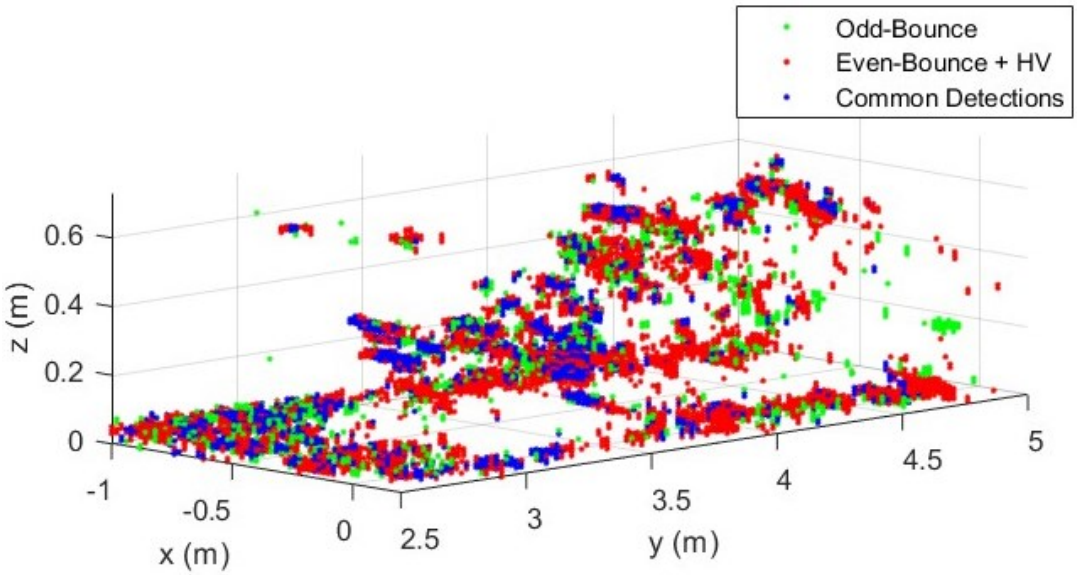

Figure 5. Sub-Nyquist aperture rendering for quarter-scale T72 tank model. Detections are shown for Odd-bounce (green), Even-Bounce + HV combination (red) and the common detection points between the two (blue).

The main features of the tank are visible, such as the turret, main body and tracks. There is significant overlap in detection between the two mechanisms. The even-bounce scattering mechanism is visibly the more dominant scattering mechanism across the tank structure.

5.2 Bistatic

The SSARVI algorithm was also applied to polarimetric bistatic data. Figure 6 presents the four point clouds for the four polarisation channels, HH, VV, HV and VH. Recall that in a bistatic configuration, HV is generally different from VH.

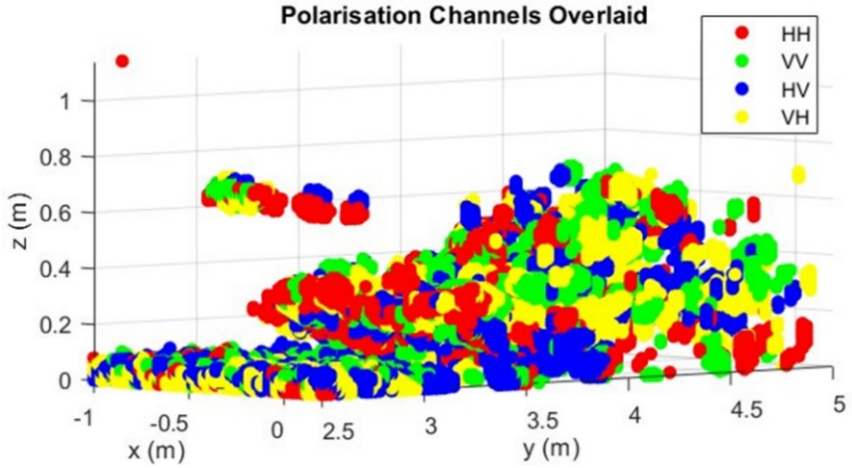

Figure 6: Sub-Nyquist SAR aperture linear polarization detections for bistatic data collection.

The sparse SAR aperture employed is shown in Figure 2b). It consists of 12 horizontal linear passes of the transmitter, with a fixed receiver position. The passes are necessarily unevenly distributed in height with a normalized standard deviation of 0.6. The aperture has a maximum inter-pass spacing of 22.5 cm. For a 1.8 m Volume of Interest (VoI), the sparse sampling corresponds to a vertical sampling rate of 36% below full Nyquist, assuming a uniformly sampled target scene.

Very few detection artefacts are present, and no vertical aliasing artefacts are evident as would be the case with conventionally formed images with this sparse aperture sampling.

6 CONCLUSIONS

Three-dimensional polarization decomposed point clouds have been formed from sparse aperture SAR laboratory measurement data. The SSARVI algorithm was applied both to linear polarization channels independently, and to Pauli polarimetric decompositions, allowing composite point cloud distributions plots to be presented. Similar detection performances were achieved for the decompositions as for previous single polarimetric channel investigations[8], achieving similar results for 36% below aperture Nyquist sampling employed.

Both the monostatic and bistatic results show that for the complex target investigated, different polarimetric channels and decompositions provide different detection point clouds, so that when these are combined, the target surface is more clearly defined.

Preliminary results show that polarimetric features can be readily classified with the point clouds for simple targets, in particular the sphere and various sphere multipath scattering artefacts, however for the complex target, the association of the polarimetric decomposition with scattering mechanism is difficult to determine.

Future research will involve combining multiple bistatic collections, emulating a sparse multistatic collection from a multistatic SAR drone swarm or satellite constellation. Additional polarimetric decompositions are to be investigated, in particular those likely to be physically meaningful for bistatic generalisations[15,16,17,18,19].

7 REFERENCES

1. Moreira A, Prats-Iraola P, Younis M, Krieger G, Hajnsek I, Papathanassiou KP. A tutorial on synthetic aperture radar. IEEE Geosci Remote Sens Mag. 2013;1(1):6–43. doi: 10.1109/MGRS.2013.2248301.
2. André D. An analysis of 3D SAR from single pass nonlinear radar platform trajectories. In: Algorithms for Synthetic Aperture Radar Imagery XVII. SPIE; 2010. p. 769908.
3. Elgy J, Andre D, Finnis M. Volumetric SAR near-field upsampling and basebanding. Electron Lett. 2020;56(12):622–624. doi: 10.1049/el.2019.4123.
4. Baselice F, Ferraioli G, Pascazio V. Three dimensional reconstruction using COSMO-SkyMed high-resolution data. In: 2011 Microwaves, Radar and Remote Sensing Symposium, MRRS-2011 - Proceedings. 2011. p. 161–164.
5. Xu G, Zhang B, Yu H, Chen J, Xing M, Hong W. Sparse Synthetic Aperture Radar Imaging From Compressed Sensing and Machine Learning: Theories, applications, and trends. IEEE Geosci Remote Sens Mag. 2022;10(4):32–69. doi: 10.1109/MGRS.2022.3218801.
6. Carande R, Cohen D. SAR Point Cloud Generation System. United States: U. S. Patent Office; 2014. WO/2014/074631.
7. Woollard M, Blacknell D, Griffiths H, Ritchie MA. SARCASTIC v2.0—High-Performance SAR Simulation for Next-Generation ATR Systems. Remote Sens (Basel). 2022;14(11):2561. doi: 10.3390/rs14112561.
8. Welsh R, Andre D, Finnis M. Volumetric interferometry for sparse 3D synthetic aperture radar with bistatic geometries. Electron Lett. 2023;59(12). doi: 10.1049/ell2.12851.
9. Ren H, Sun Z, Yang J, Xiao Y, An H, Li Z, et al. Swarm UAV SAR for 3-D Imaging: System Analysis and Sensing Matrix Design. IEEE Transactions on Geoscience and Remote Sensing. 2022;60. doi: 10.1109/TGRS.2022.3221775.
10. Krieger G, Hajnsek I, Papathanassiou KP, Younis M, Moreira A. Interferometric synthetic aperture radar (SAR) missions employing formation flying. Proceedings of the IEEE. 2010;98(5):816–843. doi: 10.1109/JPROC.2009.2038948.

11. Airbus Space. Airbus to develop technology for ultra-high-resolution satellites for UK MOD. Available from: https://www.airbus.com/en/newsroom/press-releases/2019-09-airbus-to-develop-technology-for-ultra-high-resolution-satellites. Accessed 2023 Aug 8.
12. Cloude R, Pottier E. Review of Target Decomposition ar Polarimetry. 1996.
13. Saville MA, Jackson JA, Fuller DF. Rethinking vehicle classification with wide-angle polarimetric SAR. IEEE Aerospace and Electronic Systems Magazine. 2014;29(1):41–49. doi: 10.1109/MAES.2014.130057.
14. Germond A-L, Pottier E, Saillard J. FOUNDATIONS OF BISTATIC RADAR POLARIMETRY THEORY. In: Radar Conference. 1997.
15. Titin-Schnaider C. Physical meaning of bistatic polarimetric parameters. IEEE Transactions on Geoscience and Remote Sensing. 2010;48(5):2349–2356. doi: 10.1109/TGRS.2009.2038063.
16. Titin-Schnaider C. Characterization and recognition of bistatic polarimetric mechanisms. IEEE Transactions on Geoscience and Remote Sensing. 2013;51(3):1755–1774. doi: 10.1109/TGRS.2012.2208118.
17. Titin-Schnaider C. Polarimetric characterization of bistatic coherent mechanisms. IEEE Transactions on Geoscience and Remote Sensing. 2008;46(5):1535–1546. doi: 10.1109/TGRS.2008.916078.
18. Andre D, Welsh R, Finnis M. Laboratory Multistatic Polarimetric 3D SAR. 2022.
19. Andre D, Sabiers R, Finnis M. Through-Wall Multistatic Polarimetric 3D SAR. 2021.